

Extended Brinkman-Rice Picture and Its Application to High- T_c Superconductors*

Hyun-Tak Kim[†]

Telecom. Basic Research Lab., ETRI, Taejon 305-350, Korea

Abstract

This is a full-paper of the paper(Physica C341-348, 259(2000)) published previously. The effective charge and Coulomb energy are justified by means of measurement. Theoretical calculations of the effective mass depending on band filling also are given by Gutzwiller's variational calculations. On the basis of the concept of measurement, the effective mass is an average of the true effective mass in the Brinkman-Rice(BR) picture for metal phase and is the effect of measurement. The true correlation strength ($U/U_c = \kappa_{BR}$) in the BR picture is evaluated as $0.92 < \kappa_{BR} < 1$ for YBCO. High- T_c superconductivity is attributed to the true effective mass (regarded as the density of states) caused by the large κ_{BR} value. Furthermore, the validity of the BR picture is indirectly proved through the extended BR picture.

1 Introduction

Several theoretical studies have been performed to reveal the mechanism of the metal-insulator transition (MIT) in $3d$ transition-metal oxides including strongly correlated high- T_c superconductors[1–6]. Mott first introduced the concept of the Mott MIT of the first order (called "Mott transition"), which is caused by a strong on-site Coulomb repulsion U [1]. Hubbard[2] made a model which explained the splitting between the lower and upper Hubbard bands resulting in increased U , which is indicative of an insulator and second-order MIT. However, Hubbard's model has not clarified the single-particle spectral function $\rho(\omega)$ characterizing physical properties, particularly on the metallic side of the Mott transition.

*This was presented at NATO Advanced Research Workshop on New Trends in Superconductivity held at Yalta in Ukraine at Sept. 16-20 of 2001 and will be published in NATO ARW series by (Kluwer Academic Pub., edited by J. Annett and S. Kruchinin, 2001).

[†]kimht45@hotmail.com. htkim@etri.re.kr..

Brinkman and Rice[3] took account of first order MIT from results calculated using the Gutzwiller variational theory[7] under the condition of equal numbers of spin-up electrons and spin-down electrons, restricted to a metal with the electronic structure of one electron per atom. They predicted that the effective mass of a quasiparticle diverges and a MIT of first order occurs at $U/U_c=1$, and that the width of the kinetic energy decreases as $U/U_c \rightarrow 1$. These results were built on the Fermi liquid theory and have been called the Brinkman-Rice (BR) picture. However, the BR picture does not give exact information on the band-filling dependence of the effective mass.

The $d = \infty$ Hubbard model suggested that the second-order MIT occurs at $U/U_c=1$, and that the metallic side exhibits the BR picture[4]. The one-dimensional(1-D) $t - J$ model[5] and the 2-D Hubbard model[6] accounted for the band-filling dependence of the effective mass of a quasiparticle for strongly correlated metals.

On the basis of these theories, many experiments have been carried out to clarify MITs. Systematic experimental studies on MITs and the effective mass of quasiparticles have been made on filling-controlled systems[8 – 11, 16, 17]. For $\text{Sr}_{1-x}\text{La}_x\text{TiO}_3$, the sharp first-order MIT and the critical effective mass were observed near $x=0.95$ [8]. $\text{Sr}_{1-x}\text{La}_x\text{TiO}_3$ seemed to follow the BR picture, $t - J$, and 2-D Hubbard models near the Mott transition[8, 9]. However, the band-filling dependence of the effective mass has not been explained quantitatively[8, 9].

Morikawa et al.[12], by analyzing the photoemission spectra, suggested that metallic properties for CaVO_3 and SrVO_3 metals are governed by long-range interaction as well as short-range interaction. Inoue et al.[13] and Makino et al.[14], by controlling the bandwidth, reported that the effective mass for $\text{Ca}_{1-x}\text{Sr}_x\text{VO}_3$ metals did not increase critically near the Mott transition. These analyses differ from those of models based on short-range interaction. One cause of the difference is because the band-filling dependence of the effective mass is left unspecified.

With regard to the high- T_c superconductor $\text{La}_{2-x}\text{Sr}_x\text{CuO}_4$, the parent material La_2CuO_4 has been known to be an antiferromagnetic Mott insulator, although any behavior indicative of the first-order transition has not been observed near $x=0$. The effective mass of a quasiparticle increases with increasing x in the underdoped regime[18]. This La-system seems to be explained by the Hubbard models rather than the BR picture, $t - J$, or 2-D Hubbard models exhibiting first-order transition. Up to now, there is no theory capable of explaining the MITs of both $\text{Sr}_{1-x}\text{La}_x\text{TiO}_3$ and $\text{La}_{2-x}\text{Sr}_x\text{CuO}_4$ systems.

On the generic question of high- T_c superconductivity, since discovering the high- T_c superconductor, the van Hove singularity (vHs), which is a 2D-density of states(DOS), has been suggested as an explanation for the high- T_c mechanism;

the 2D-DOS is proportional to the effective mass of a quasiparticle. However, through experimental results, many researchers have pointed out that the vHs is unfit to account for high- T_c superconductivity[19 – 23]. Instead, an extended vHs has been observed by angle-resolved photoemission spectroscopy[24, 25]. This extended vHs may be a power law as a function of the difference between the extended saddle-point energy and the Fermi energy. The band-filling dependence of the 2D-DOS regarded as the extended vHs still remains to be clarified by theory. The mechanism of a pseudogap for the underdoped regime for superconductors has long been discussed[26 – 30]. A new phase diagram suggested that the pseudogap disappears at optimal doping [31].

In this paper, in order to reveal the above problems, first of all, we review the paper which gives an insight regarding the extension of the Brinkman-Rice picture and shows experimental results[32]. The concept of measurement is introduced to justify the effective Coulomb energy based on the metal-insulator instability derived from the charge-density-wave(CDW) theory of BaBiO₃. Theoretical calculations of the effective mass also are given. Other examples not given in the paper, including data on high- T_c superconductivity and strongly correlated materials, are appended, for the extended BR picture.

2 Extended Brinkman-Rice picture

2.1 Justification of the effective Coulomb energy

A strongly correlated metallic system with a s band structure is assumed for a $d = \infty$ dimensional simple-cubic lattice. Let n and l be the number of electrons (or carriers) and the number of atoms (or lattices), respectively. In the case of one electron per atom, *i.e.*, $n = l$, the metallic system is a metal and the existence probability ($P = n/l = \rho =$ band filling) of electrons on nearest-neighbor sites is one. The electrons have a spin on an atom. The on-site Coulomb repulsion is always given by $U = U' \equiv \langle \frac{e^2}{r} \rangle$, as shown in Fig. 1 (a). However, in the case of $n < l$ which occurs by doping an element to a base insulator or metal, U is determined by probability. The metallic system is quite complicated, as shown in Fig. 1 (b). Four types of regions for the system can be distinguished as possible extreme examples. Region A in Fig. 1 (b) has no electrons on its atomic sites, which corresponds to a normal insulator. Region C has a metallic structure of one electron per atom. Regions B and D have a charge-density-wave (CDW) structure unlike the assumed cubic lattice. Electrons in region D have opposite spins. This must be regarded as a CDW insulator with the CDW-energy gap depending on the local CDW-potential energy[33, 34]. Moreover, even when one electron on an atom is removed, the nearest-neighbor sites of the atom without an

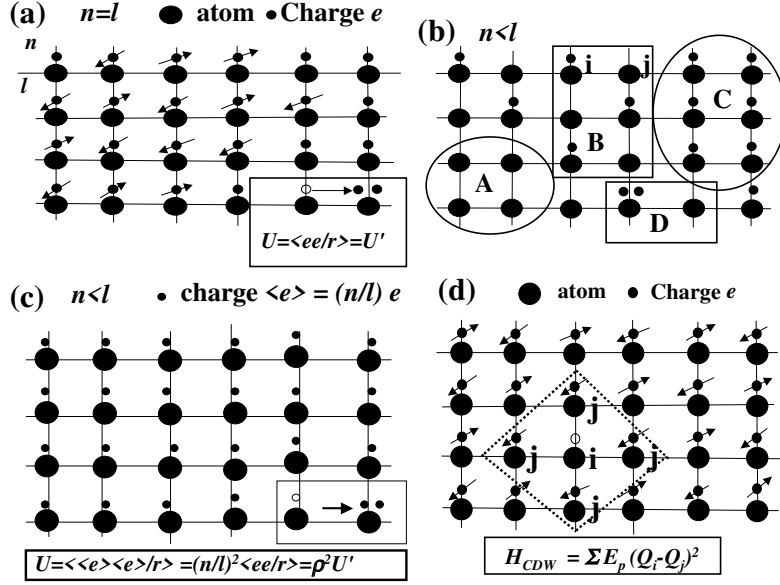


Figure 1: (a) In the case of one electron per atom, the on-site Coulomb repulsion is given as $U = \langle \frac{e^2}{r} \rangle = U'$. (b) In the case of $n < l$, the four possible electronic structures are region A (insulator), region C (metal), and regions B and D (CDW insulators). Here, n and l denote the number of carriers in region C and the number of atoms in the whole system, respectively. (c) In the case of less than one electron per atom, the on-site Coulomb repulsion is given as $U = (n/l)^2 \langle \frac{e^2}{r} \rangle = \rho^2 U'$. (d) In the case where one electron is removed, both an atom i and the nearest neighbors j of the atom become the CDW insulator due to charge disproportionation, $\delta Q = Q_i - Q_j$.

electron and the atom itself are regarded as region B, as shown in Fig. 1(d). The potential energy can be interpreted as a potential for impurities in the metallic system.

The CDW-potential energy, $V_{CDW} = -E_p(Q_i - Q_j)^2$, is derived by breathing-mode distortion due to the charge disproportionation ($\delta Q = Q_i - Q_j$) between nearest-neighbor sites, where Q_i and Q_j are charges irrespective of spins on i and j sites, respectively. The CDW gap is regarded as a pseudogap (or pinned CDW gap), and can be observed by optical methods[26 – 30], photoemission spectroscopy[27], and heat capacity measurement[35, 36] for high- T_c superconductors. The pseudogap occurs if the number of carriers is less than the number of atoms. Therefore, the metallic system is inhomogeneous and cannot be self-consistently represented in k -space, *i.e.*, U and the density of states of the system

are not given. To overcome this difficulty, carriers on atoms in the metal phase (region C) have to be averaged over sites, as shown in Fig. 1 (c). The on-site effective charge is $Q_i = Q_j = \langle e \rangle = (n/l)e = \rho e$, on average over sites. The metallic system, then, can act as a metal, because $V_{CDW} = 0$ due to $\delta Q = 0$. Therefore, the effective Coulomb energy is given by $U = \rho^2 U'$, as shown in Fig. 1 (c).

To illustrate the physical meaning of $P = (\langle e \rangle / e) = \rho < 1$, then $\mu \ll 1$, $\rho = 1 - \mu < 1$, where $\mu = 1 - \rho = n_b/l$ (or $n_b = l - n$), n_b is the number of bound charges bound by V_{CDW} [34]. For the CDW insulating side, $\mu \ll 1$ indicates that there are a few doubly occupied atoms, such as in region D. For the metallic side, $\rho < 1$ indicates that a number of carriers exist. This suggests that region C is extremely wide.

The insulating and metallic sides correspond to two phases, which are attributed to the metal-insulator instability (or instability of the CDW-potential energy)[34] at $\rho=1$ (half filling). This indicates that a metal (perfect single phase) with the electronic structure of Fig. 1 (a) is not synthesized. Junod et al.[37] suggested that even the best samples are not 100% superconducting, which supports the metal-insulator instability[34]. Thus, synthetic metals composed of several atoms always have the electronic structure of two phases, such as Fig. 1 (b), which is a necessity of the development of $\langle e \rangle = \rho e$.

To justify the fractional charge of carriers in the metallic system with two phases, the concept of measurement is necessary. When measuring the charge of carriers in the metallic system of Fig. 1 (b), the measured charge becomes the effective fractional one, $\langle e \rangle = \rho e$, representing the average meaning of the system. This is because experimental data for the metallic system are expectation values of statistical averages. When *not* measuring charge, the charge of carriers in region C in Fig. 1 (b) remains the true elementary charge, not observed by means of measurement.

Accordingly, for the metallic system where $n \leq l$, the effective fractional Coulomb energy, $U = \rho^2 U'$, is defined by using $\langle e \rangle = \rho e$ and justified by means of measurement.

Additionally, although the justification is based on the metal insulator instability derived from the CDW theory, it can be applied to all strongly correlated metals including cuprate superconductors. This is because there is much experimental evidence for the CDW in cuprate superconductors although their parent materials are antiferromagnetic insulators, which is shown in a review paper[38].

2.2 Calculation of the effective mass

For the metallic system regarded as a real synthetic metal with an electronic

structure such as Fig. 1 (b), the effective mass of quasiparticles needs to be calculated. Hamiltonians of the metallic system can be considered as follows. Hamiltonian, H , is given by

$$H = H_1 + H_2, \quad (1)$$

$$H_1 = \sum_k (a_{k\uparrow}^\dagger a_{k\uparrow} + a_{k\downarrow}^\dagger a_{k\downarrow}) \epsilon_k + U \sum_g a_{g\uparrow}^\dagger a_{g\downarrow}^\dagger a_{g\downarrow} a_{g\uparrow}, \quad (2)$$

$$H_2 = - \sum_{i,j} E_p (Q_i - Q_j)^2, \quad (3)$$

where $a_{k\uparrow}^\dagger$ and $a_{g\uparrow}^\dagger$ are the creation operators for electrons in the Bloch state k and the Wannier state g , respectively, and ϵ_k is the kinetic energy when $U=0$. H_1 and H_2 are Hamiltonians of the metallic region C and the CDW-insulator regions B and D, respectively. In the case of Fig. 1 (a) and (c), the Hamiltonian is reduced to H_1 because H_2 disappears due to $\delta Q = 0$, and the on-site Coulomb energy is given by $U = \rho^2 U'$. H_1 is consistent with the Hamiltonian used in the Gutzwiller variational theory[7].

In order to calculate the effective mass of quasiparticles and the ground-state energy for a strongly correlated metallic system, the Gutzwiller variational theory[7, 39 – 41] is used. H_1 is supposed to describe the metallic system. The wave function is written as

$$|\Psi\rangle = \eta^{\bar{\nu}} |\Psi_0\rangle, \quad (4)$$

where $|\Psi_0\rangle$ is the wave function when $U = 0$, $\bar{\nu}$ is the number of doubly occupied atoms, and $0 < \eta < 1$ is variation. The expectation value of H_1 is regarded to be

$$\langle H \rangle = \frac{\langle \Psi | \sum_{ij} \sum_{\sigma} t_{ij} a_{i\sigma}^\dagger a_{j\sigma} | \Psi \rangle + \langle \Psi | U \sum_i \rho_{i\uparrow} \rho_{i\downarrow} | \Psi \rangle}{\langle \Psi | \Psi \rangle}. \quad (5)$$

The second part of the equation is simply given by $\langle \Psi | U \sum_i \rho_{i\uparrow} \rho_{i\downarrow} | \Psi \rangle = U \bar{\nu}$ because $|\Psi_0\rangle$ is an eigenstate of the number operator $\sum_i \rho_{i\uparrow} \rho_{i\downarrow}$. The first part is dealt with by assuming that the motion of the up-spin electrons is essentially independent of the behavior of the down-spin particles (and *vice versa*). By minimization with respect to η , Gutzwiller obtained an extremely simple result for the ground-state energy, namely,

$$E_g/l = q_\uparrow(\bar{\nu}, \rho_{i\uparrow}, \rho_{i\downarrow}) \bar{\epsilon}_\uparrow + q_\downarrow(\bar{\nu}, \rho_{i\uparrow}, \rho_{i\downarrow}) \bar{\epsilon}_\downarrow + U \bar{\nu}. \quad (6)$$

Here,

$$\bar{\epsilon}_\sigma = l^{-1} \langle \Psi | \sum_{ij} t_{ij} a_{i\sigma}^\dagger a_{j\sigma} | \Psi \rangle = \sum_{k < k_F} \epsilon_k < 0 \quad (7)$$

is the average energy of the σ spins without correlation and ϵ_k is the kinetic energy in H_1 , with the zero of energy chosen so that $\sum_k \epsilon_k = 0$. $\bar{\epsilon}_\uparrow$ is equal to $\bar{\epsilon}_\downarrow$.

The discontinuities, q_σ , in the single-particle occupation number at the Fermi surface are given by

$$q_\sigma = \frac{\left(\sqrt{(\rho_\sigma - \bar{\nu})(1 - \rho_\sigma - \rho_{-\sigma} + \bar{\nu})} + \sqrt{(\rho_{-\sigma} - \bar{\nu})\bar{\nu}}\right)^2}{\rho_\sigma(1 - \rho_\sigma)}, \quad (8)$$

where $\rho_\sigma = \frac{1}{2}\rho$, $0 < \rho \leq 1$ and $\rho_\uparrow = \rho_\downarrow$ [39,40]. This, calculated by Ogawa et. al.[39] who simplified the Gutzwiller variational theory, is in the context of the Gutzwiller variational theory. Eq. (8) is a function of ρ_σ and $\bar{\nu}$ irrespective of the quantity of charges. This can be analyzed in two cases of $\rho=1$ and $0 < \rho < 1$, because Gutzwiller did not limit the number of electrons on an atom for the metallic system.

In the case of $\rho=1$,

$$q_\sigma = 8\bar{\nu}(1 - 2\bar{\nu}). \quad (9)$$

This was described in the BR picture.

In the case of $0 < \rho < 1$, two kinds of q_σ can be considered. One is Eq. (8) when the electronic structure is $\delta Q \neq 0$, as shown in Fig. 1 (b). However, Eq. (8) can not be applied to the metallic system, as mentioned in the above section. The other is Eq. (9) when the electronic structure is $\delta Q=0$, as shown in Fig. 1 (c). Eq. (9) is obtained from substituting ρ_σ in Eq. (8) with ρ'_σ . Here, $\rho' = (n'/l) = 1$ and $\rho'_\sigma = \frac{1}{2}$, because the number of the effective charges, n' , is equal to l . It should be noted that the metallic system with less than one electron per atom, as shown in Fig. 1 (c), is mathematically consistent with that with one electron per atom, as shown in Fig. 1 (a).

Although the following calculations were performed by Brinkman and Rice, the calculations are applied to the effective mass. In the case of Fig. 1 (c), by applying Eq. (9) to Eq. (6) and by minimizing it with respect to $\bar{\nu}$, the number of the doubly occupied atoms is obtained as

$$\begin{aligned} \bar{\nu} = \frac{1}{4}\left(1 + \frac{U}{8\bar{\epsilon}}\right) &= \frac{1}{4}\left(1 - \frac{U}{U_c}\right), \\ &= \frac{1}{4}(1 - \kappa\rho^2), \end{aligned} \quad (10)$$

where $U_c=8|\bar{\epsilon}|$ because of $\bar{\epsilon} = \bar{\epsilon}_\uparrow + \bar{\epsilon}_\downarrow < 0$, $U = \rho^2 U'$ and $U' = \kappa U_c$. $0 < \kappa \leq 1$ is the correlation strength. By applying Eq. (10) to Eq. (9) again, the effective mass

is given by

$$\begin{aligned} q_\sigma^{-1} = \frac{m^*}{m} &= \frac{1}{1 - (\frac{U}{U_c})^2}, \\ &= \frac{1}{1 - \kappa^2 \rho^4}. \end{aligned} \quad (11)$$

Although the separate conditions are $0 < \rho \leq 1$ and $0 < \kappa \leq 1$, m^* is defined under the combined condition $0 < \kappa \rho^2 < 1$ and is an average of the true effective mass in the BR picture for metal phase (region C in Fig. 1 (b)). Eq. (11) is shown in Fig. 2(a). The effective mass increases as it approaches $\kappa=1$ and $\rho=1$. For $\kappa \neq 0$ and $\rho \rightarrow 0$, the effective mass decreases and, finally, the metallic system undergoes a normal (or band-type) metal-insulator transition; this transition is continuous. The system at $\kappa \rho^2 = 1$ can be regarded as the insulating state which is the paramagnetic insulator because $\bar{\nu} = 0$. At a κ value (not one), the MIT from a metal at a ρ value of just below $\rho=1$ to the insulator at both $\rho=1$ and $\kappa=1$ is the first-order transition on band filling. This has been called the Mott transition by a lot of scientists including author. However, this is theoretically not the Mott transition which is a first-order transition from a value of U to U_c in a metal with the electronic structure of one electron per atom at $\rho=1$, as given in the BR picture. The Mott transition does not occur in real crystals because a perfect single-phase metal with $\rho=1$ is not made. Conversely, by hole doping (or electron doping to a metallic system with hole carriers) of a very low concentration, the first-order transition from the insulator with $\bar{\nu}=0$ to a metal can be interpreted as an abrupt breakdown of the balanced critical Coulomb interaction, U_c , between electrons. Then, the U_c value in the insulator reduces to a U value in a metal phase and an insulating phase produces due to doping of opposite charges, as shown in Fig. 1(d). This first-order transition with band filling is very important result found in this picture, which differs from the continuous (Mott-Hubbard or second-order) transition by a large U given by the Hubbard theory.

In order to obtain the expectation value of the energy in the (paramagnetic) ground state, Eqs. (10) and (11) are applied to Eq. (6). E_g is given by

$$E_g/l = \bar{\epsilon}(1 - \kappa \rho^2)^2. \quad (12)$$

As $U/U_c = \kappa \rho^2$ approaches one, E_g goes to zero.

In addition, the spin susceptibility in the BR picture is replaced by

$$\chi_s = \frac{m^*}{m} \frac{\mu_B^2 N(0)}{(1 - \frac{1}{2} N(0) \kappa \rho^2 U_c \frac{1 + \frac{1}{2} \kappa \rho^2}{(1 + \kappa \rho^2)^2})}, \quad (13)$$

where $N(0)$ is the density of states at the Fermi surface and μ_B is the Bohr magneton. The susceptibility is proportional to the effective mass which allows the enhancement of χ_s .

In such a case, m^* , E_g/l and χ_s are the averages of true effective values in region C in Fig. 1 (b), which is described by the BR picture, and are justified only by means of measurement. The true effective values in the BR picture are not measured experimentally, as mentioned previously. In particular, the magnitude of the true effective mass in the BR picture has the same value regardless of the extent of region C, while the measured effective mass depends upon the extent of region C. Furthermore, validity of the BR picture and the Mott transition was also discussed by theorists[42, 43], which is because the BR picture has not been proved experimentally. However, the validity is indirectly proved through the above picture.

3 Application to strongly correlated metals

This section describes the application of the effective mass to experimental data of strongly correlated metals. $\text{Sr}_{1-x}\text{La}_x\text{TiO}_3$ may be one of the most desirable systems in which the critical dependence of physical parameters on the band filling can be investigated in the vicinity of the MIT. For $\text{Sr}_{1-x}\text{La}_x\text{TiO}_3$, the number of $3d$ electrons varies from 0 to 1 with a change of x from SrTiO_3 to LaTiO_3 . The final compound LaTiO_3 is transformed to a metallic state with a slight increase in $x \geq 0.05$. Tokura et al.[8] and Kumagai et al.[9] measured the resistivity, the magnetic susceptibility, the Hall coefficient R_H , and the low-temperature heat capacity as a function of x for $\text{Sr}_{1-x}\text{La}_x\text{TiO}_3$. The absolute value of R_H^{-1} increases linearly with x up to at least $x=0.95$. The band filling ρ corresponds to x because the number of doped carriers with x agrees with the data for carriers obtained from the Hall coefficient. The heat capacity in Fig. 3 of reference 8 is replotted, as shown in Fig. 2 (b). The effective mass of Eq. (11) closely follows the heat-capacity data where $\kappa=1$. The heat capacity increases with x and peaks at $x=0.95$. The first-order transition is found between $x=0.95$ and $x=1$, which is not the Mott transition defined by theory but the transition with band filling. Tokura et al.[8] and Kumagai et al.[9] suggested that the increase of the heat capacity with x is due to an enhancement of the effective mass of correlated electrons, although the carrier density increases with x ; the coefficient, γ , of the heat capacity is proportional to the effective mass in the Fermi Liquid theory. Moreover, the large effective mass was also observed by optical methods[10] and nuclear-magnetic-resonance experiments[11].

Where $x < 0.95$, $\kappa=1$ in Fig. 2(b) indicates that the true effective mass has

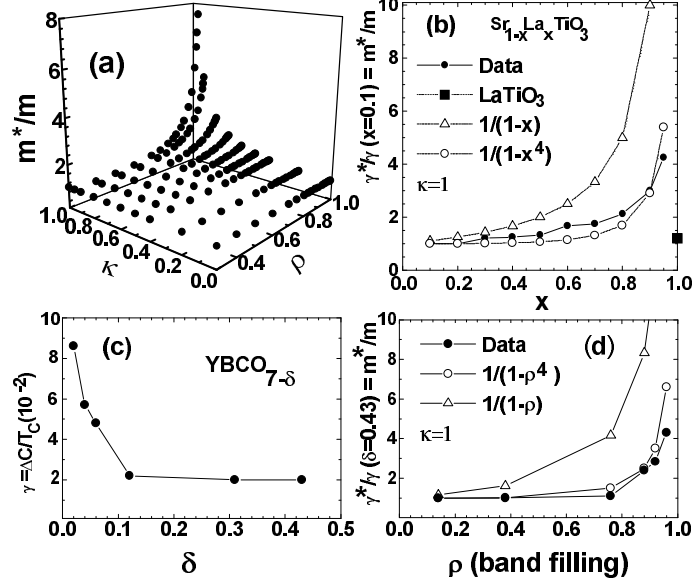


Figure 2: (a) The effective mass, $\frac{m^*}{m} = \frac{1}{1-\kappa^2\rho^4}$. (b) Experimental data (\bullet) of the heat capacity for $\text{Sr}_{1-x}\text{La}_x\text{TiO}_3$ presented by Tokura[8] and Kumagai[9], and a comparison between $\frac{m^*}{m} = \frac{1}{1-x^4}$ (\circ) and $\frac{m^*}{m} = \frac{1}{1-x}$ calculated from the $t - J$ model[5] (\triangle) and the Hubbard model[6] on a square lattice. Here, ρ corresponds to x because the number of quasiparticles with x agrees with that of quasiparticles obtained from the Hall coefficient[8]. Here, $\kappa=1$ and $0 < \kappa\rho^2 < 1$. (c) The heat-capacity coefficient ($\Delta c/T_c$) obtained by magnetic measurements for $\text{YBa}_2\text{Cu}_3\text{O}_{7-\delta}$ superconductors by Daümling[48]. (d) In cases where $\delta=0$ and $\delta=0.45$, the band is assumed to be full where $\rho=1$ and empty where $\rho=0$, respectively. Thus $\rho=1-\delta/0.45$. Here, $\kappa=1$ and $0 < \kappa\rho^2 < 1$. The above data were cited in reference 32.

a constant value even though the extent of region C in Fig. 1 (b) changes. The increase of x up to $x=0.95$ corresponds to the increase of region C. Because region C is described by the BR picture, the correlation strength of the BR picture, κ_{BR} , can be found. When it is assumed that the extent of the metal phase (region C) at $x=0.95$ is approximately the same as that at $x=\rho=1$, a value of $m^*/m = 1/(1-\rho^4)$ at $\rho=0.95$ and $\kappa=1$ is approximately equal to that of $m^*/m = 1/(1-\kappa_{BR}^2)$ in the BR picture. Thus, $\kappa_{BR} = (0.95)^2=0.90$ is obtained, which indicates that $\text{La}_{1-x}\text{Sr}_x\text{TiO}_3$ is very strongly correlated. Moreover, the decrease of the effective mass from $x=0.95$ to $x=0$ is not the true effect, but the effect of measurement.

For another correlated metal, $\text{Y}_{1-x}\text{Ca}_x\text{TiO}_3$, Kumagai et al.[9] obtained the same result as for $\text{Sr}_{1-x}\text{La}_x\text{TiO}_3$. In V_{2-y}O_3 , Carter et al.[16] suggested that the effective mass may diverge at the Mott MIT under pressure and decrease

as the MIT is approached with y . The MIT with y corresponds exactly to a band-type MIT in this extended BR picture. McWhan et al.[17] observed the sharp Mott MIT in Cr-doped V_2O_3 at room temperature as functions of both Cr concentration and pressure. The sharp Mott MIT is not the Mott transition in the BR picture, but the first-order transition with band filling ρ in the extended BR picture. As another experimental result, Khan et al.[44] observed the first-order transition at $x=0.02$ for h - $BaNb_xTi_{1-x}O_3$, which may also be in this context.

Morikawa et al.[12] measured the decrease of the spectrum intensity in the photoemission spectrum in going from $SrVO_3$ to $CaVO_3$, which corresponds to an increase in U/W on the basis of the Hubbard models. Here the increase of U/W indicates an increase of κ with $\rho = 1$, using the notations of the extended BR picture. The decrease of the spectrum intensity is different from the spectral function of the $d = \infty$ Hubbard model[4], which suggests band narrowing rather than a decreasing spectrum. Thus, they concluded that the effect of long-range Coulomb interaction, which limits the mass enhancement or band narrowing near the Mott transition, is much larger than that of short-range interactions. However, in this extended BR picture, the decrease of the spectrum intensity is interpreted as a decrease of U due to decreasing ρ rather than increasing U/W ($=\kappa$, $\rho = 1$). Thus, the effective mass of quasiparticles decreases in going from $SrVO_3$ to $CaVO_3$, which indicates that region C in Fig. 1 (b) gets small. The transition with x for $Ca_{1-x}Sr_xVO_3$ more closely resembles a band-type MIT than the Mott MIT although the theoretical analysis[4] regards the transition as a Mott transition, because any behavior indicative of a first-order transition due to a large U is not found. The difference between the extended BR picture and the $d = \infty$ Hubbard model is discussed in Physic C or cond-mat/0001008 in reference 32.

Inoue et al.[13] and Makino et al.[14] tried to control the bandwidth W , assuming that the number of quasiparticles does not vary with x for single crystals of $Ca_{1-x}Sr_xVO_3$. However, investigations of the BR feature near the Mott transition showed that the bandwidth did not change[12]. Instead, for high-resolution photoemission spectra, the spectral intensity corresponding to quasiparticles decreased near the Fermi energy[12]. This differs from the assumption of Inoue et al. and Makino et al..

Ahn et al.[45] investigated optical properties of (Ca, Sr)RuO₃ films on the borderline of metal-insulator transition, on the basis of the dynamical mean field theory(DMFT)[46] regarded as the $d = \infty$ Hubbard mode. The effective mass of quasiparticles increased with Sr concentration, although CaRuO₃ is more metallic than SrRuO₃. This is the same as the analysis for $Ca_{1-x}Sr_xVO_3$, but is different from that in the extended BR picture. Unlike in the BR picture, the number of quasiparticles is not conserved in the conduction band as U increases in the

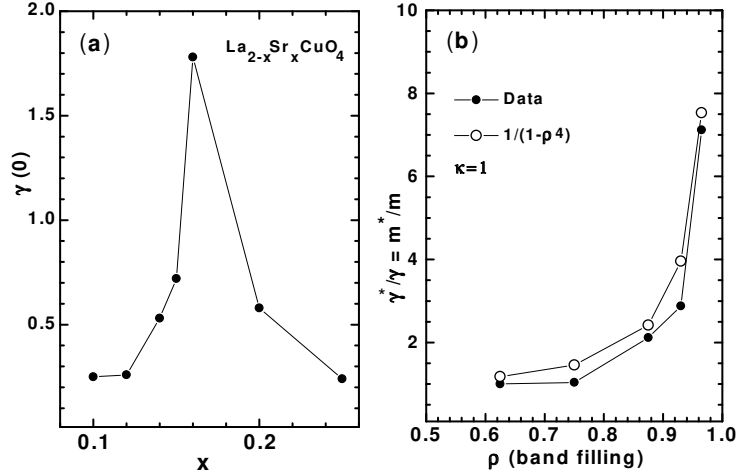


Figure 3: (a). Experimental data of the heat-capacity coefficient for $\text{La}_{2-x}\text{Sr}_x\text{CuO}_4$ superconductors presented by Y. Hongshun[47]. (b). The $m^*/m_{x=0.1}$ versus ρ is obtained from the heat-capacity coefficient value to $x = 0.1$ and an optimum doping of $x=0.16$. At $x=0.16$, the band is assumed to be half full with $\rho=1$. Thus, $\rho=x/0.16$. γ is the value of the heat capacity at $x=0.1$. The experimental data (\bullet) and $\frac{m^*}{m} = \frac{1}{1-\rho^4}$, (\circ), are shown. At $x=0.15$, the effective mass is estimated to be $m^*/m \approx 7.5$. Here, $\kappa=1$ and $0 < \kappa\rho^2 < 1$.

DMFT.

4 Application to high- T_c superconductors

This section describes the application of the extended BR picture to cuprate oxide superconductors known to be strongly correlated metals. Hongshun[47], Daümbing[48], Wühl[49], and Loram[35] observed the coefficient, γ , of the specific heat capacity, which is proportional to the effective mass corresponding to the 2D-DOS ($=\frac{m^*}{\pi\hbar^2}$). The DOS showed a jump in the specific heat capacity near optimum doping. Eq. (11) seems in line with Daümbing's data, as shown in Figs. 2 (c) and (d). The effective mass decreases with decreasing ρ , which approaches a band-type MIT. Near $\rho=1$, a behavior of singularity is shown in Fig. 2 (d). Although it is difficult to confirm whether the $\text{YBa}_2\text{Cu}_3\text{O}_{7-\delta}$ (YBCO) of $\delta=0$ at $\rho=1$ is an insulator because the effective mass near $\rho=1$ is divergent, the divergence is regarded as the first-order MIT with band filling in Eq. (11).

As for Loram's specific heat data of YBCO_{6+x} in Fig. 3 and 4 of the reference

35, the anomaly step heights, $\delta\gamma(T_c)$, agree approximately with values estimated by Daümbing and Wühl. The anomalies near $x = 0.57$ and for $x > 0.92$ have magnitudes of $\delta\gamma(T_c)/\gamma_n \approx 0.5$ and $\delta\gamma(T_c)/\gamma_n \approx 2.5$, respectively, which is closely consistent with the values observed by Daümbing. The large values of T_c and $\delta\gamma(T_c)$ with x at $x > 0.9$ showed little change. Fully oxygenated YBCO₇ was slightly overdoped, which indicates that a crystal of YBCO₇ cannot be made, and that there is an instability similar to a divergence at half filling. The instability seems related to the metal-insulator instability[34] and the divergence of the effective mass near the transition from $\rho \approx 1$ (not one) to $\rho=1$. The physical meaning of the instability indicates the transition from $\rho \neq 1$ (or inhomogeneous metallic phase or Fig. 1(b)) to $\rho=1$ (perfect homogeneous metal or Fig. 1(a)), which does not indicate the van Hove singularity. Thus, the data may be explained by the extended BR picture.

In order to evaluate the correlation strength, κ_{BR} , in the BR picture according to the same calculation method as used for La_{1-x}Sr_xTiO₃ in a previous section, when it is assumed that the extent of the metal phase (corresponding to region C) at $\rho=0.96$ and $\kappa=1$ for YBCO_{7- δ} of $\delta \approx 0.04$ is the same as that at $\rho=1$, $m^*/m = 1/(1 - \rho^4)$ at $\rho=0.96$ is approximately equal to $m^*/m = 1/(1 - \kappa_{BR}^2)$ in the BR picture. Then $\kappa_{BR} = \rho^2 = (0.96)^2 = 0.92$ is obtained, which indicates that the YBCO superconductor is strongly correlated.

In the case of La_{2-x}Sr_xCuO₄(LSCO) superconductors, the heat capacity data are applied to Eq. (11), as shown in Fig. (3). Band filling at $x=0.15$ is evaluated as $\rho=0.96$. By the same calculation method, $\kappa_{BR} = \rho^2 = 0.92$ is determined. Moreover, the ρ dependency of the effective masses, as shown in Figs. 2 and 3, is the effect of measurement. Values of the true effective masses are constant, though ρ varies. The 2D-DOS using the effective mass in Eq. (11) differs from an enhanced 2D-DOS combining both the van Hove singularity and the effect of mass enhancement[15]. The enhanced 2D-DOS did not agree with experimental data of the heat capacity at optimal doping [15]. In addition, the effective mass, as measured by the de Haas-van Alphen effect at 2.3 K for YBa₂Cu₃O_{6.97}, was found to be $m^*/m=2.8-4.4$ [50]. The cyclotron mass of the organic superconductor, (BEDT-TTF)₂Cu(NCS)₂, was found to be $m_c/m_0 \approx 3.5$ [51, 52]. These large masses might be attributed to the strong correlation in the BR picture. It is suggested here that they may well be the cause of high- T_c values for high- T_c superconductors.

To account for high- T_c superconductivity, the van Hove scenario or singularity (vHs) has been introduced. The extended saddle point near the Fermi energy has also been observed by ultra-high-energy angle-resolved photoemission spectroscopy[19, 20, 24, 25]. It has been suggested that a T_c value is dependent on

the extent (or width and intensity of spectra) of the flat band[53] at the extended saddle-point energy[19, 20, 53]. That is, the extent of the flat band, corresponding to the number of quasiparticles in the flat band, increases with increasing T_c . However, if this interpretation is correct, it conflicts with the presence of quasiparticles at the Fermi surface, as mentioned in the BR and extended-BR pictures and the heat capacity data mentioned previously. Therefore, the singularity in the effective mass is different from the extended vHs, which may be a power law as a function of the difference between the extended saddle-point energy and the Fermi energy.

A new Fermi-surface topology for the Bi-2212 system has been suggested, instead of the flat band with the hole-like Fermi surface[54, 55]. In the new topology, a main band is centered around Γ with a smaller saddle point at \bar{M} above E_F . It is described by an electron-like Fermi-surface topology different from that of the flat band. The main-band dispersion has been observed at the photon energy level of 33 eV for Bi-2212 crystals. At E_F , the single-particle spectral weight, $A(k, E_F)$, is at a peak corresponding to quasiparticles. The peak can be regarded as band filling in the effective mass as 2D-DOS. Therefore, the extent of the flat band dependent on T_c , as mentioned previously, can be interpreted as the magnitude of the weight at the Fermi energy and as the extent of region C, too. Furthermore, the new topology, such as the BR picture with quasiparticles at the Fermi surface, is within the Fermi-liquid-theory framework.

5 Conclusion

The first-order transition on band filling for $\text{Sr}_{1-x}\text{La}_x\text{TiO}_3$ (SLTO) and the experimental data of the heat capacities, $\gamma^*/\gamma=m^*/m$, for SLTO, $\text{YBCO}_{7-\delta}$, and LSCO were well correlated by the extended BR picture. The true correlation strengths in the BR picture in a metal phase (region C) were evaluated to be $0.90 \leq \kappa_{BR} < 1$ for SLTO, $0.92 \leq \kappa_{BR} < 1$ for YBCO, and $0.92 \leq \kappa_{BR} < 1$ for LSCO. The true effective mass always has a constant value regardless of the magnitude of ρ . High- T_c superconductivity is attributed to the true effective mass (regarded as the density of states) caused by the large κ_{BR} value.

The ρ dependence of the effective mass is not an intrinsic effect but one of measurement. In the general phase diagram, the parabolic- T_c curve and the declined linear of the pseudogaps are also the effect of measurement. For high- T_c superconductors, the MIT in the underdoped regime can be explained without the concept of spin interaction. Gabovich's review paper [38] may give suggestions regarding the MIT based on the density wave. Furthermore, the concept of measurement being correlated to the extended BR picture can also be applied to explain the measured physical properties of other synthetic metals or insulators.

Acknowledgements

I acknowledge Dr. Kwang-Yong Kang for providing the research environment for this research. The use of Fig. 3(a) was permitted by Elsevier Science Co..

References

- [1] N. F. Mott, Metal-Insulator Transitions Chapter 3, (Taylor& Frances, 2nd edition, 1990).
- [2] J. Hubbard, Proc. R. Soc. London A 276, 238 (1963);277, 237 (1964); 281, 401 (1964).
- [3] W. F. Brinkman and T. M. Rice, Phys. Rev. B **2**, 4302 (1970).
- [4] X. Y. Zhang, M. J. Rozenberg, and G. Kotliar, Phys. Rev. Lett. **70**, 1666 (1993).
- [5] M. Kawakami and S. K. Yang, Phys. Rev. Lett. **65**, 2309 (1990).
- [6] N. Furukawa and M. Imada, J. Phys. Soc. Jpn. **60**, 3604 (1991).
- [7] M. C. Gutzwiller, Phys. Rev. 137, A1726 (1965).
- [8] Y. Tokura, Y. Taguchi, Y. Okada, Y. Fujishima, T. Arima, K. Kumagai, and Y. Iye, Phys. Rev. Lett. **70**, 2126 (1993).
- [9] K. Kumagai, T. Suzuki, Y. Taguchi, Y. Okada, Y. Fujishima, and Y. Tokura, Phys. Rev. B **48**, 7636 (1993).
- [10] Y. Fujishima, Y. Tokura, T. Arima, and S. Uchida, Phys. Rev. B **46**, 11167 (1992).
- [11] Y. Furukawa, I. Okamura, K. Kumagai, T. Goto, T. Fukase, Y. Taguchi, and T. Tokura, Phys. Rev. B **59** 10550 (1999).
- [12] K. Morikawa, T. Mizokawa, K. Kobayashi, A. Fujimori, H. Eisaki, S. Uchida, F. Iga, and Y. Nishihara, Phys. Rev. B **52**, 13 711 (1995).
- [13] I. H. Inoue, O. Goto, H. Makino, N. E. Hussey, and M. Ishikawa, Phys. Rev. B **58**, 4372 (1998).
- [14] H. Makino, I. H. Inoue, M. J. Rozenberg, I. Hase, Y. Aiura, and S. Onari, Phys. Rev. B **58**, 4384 (1998).
- [15] C. C. Tsuei, C. C. Chi, D. M. Newns, P. C. Pattnaik, and M. Daumling, Phys. Rev. Lett. **69**, 2134 (1992).
- [16] S. A. Carter, T. F. Rosenbaum, P. Metcalf, J. M. Honig, and J. Spal, Phys. Rev. B **48**, 16841 (1993).
- [17] D. B. McWhan, T. M. Rice, and J. P. Remeika, Phys. Rev. Lett. **23**, 1384 (1969).:D. B. McWhan, A. Menth, J. P. Remeika, W. F. Brinkman, and T. M. Rice, Phys. Rev. B **7**, 1920 (1973).
- [18] N. Momono, M. Ido, T. Nakano, M. Oda, Y. Okajima, and K. Yamaya, Physica C **233**, 395 (1994).
- [19] D. M. King, Z. X. Shen, D. S. Dessau, D. S. Marshall, C. H. Park, W. E. Spicer, J. L. Peng, Z. Y. Li, and R. L. Greene, Phys. Rev. Lett. **73**, 3298 (1994).
- [20] T. Yokoya, A. Chainani, T. Takahashi, H. Ding, J. C. Campuzano, H. K. Yoshida, M. Kashi, and Y. Tokura, Phys. Rev. B **54**, 13311 (1996).
- [21] J. L. Tallon and C. Bernhard, Phys. Rev. Lett. **75**, 4552 (1995).
- [22] J. L. Tallon, G. V. Williams, C. Bernhard, D. M. Pooke, M. P. Staines, J. D.

- Johnson, and R. H. Meinhold, Phys. Rev. B **53**, R11972 (1996).
- [23] D. Y. Xing, M. Liu, and C. D. Gong, Phys. Rev. B, **44**, 12525 (1991).
- [24] K. Gofron, J. C. Campuzano, A. A. Abrikosov, M. Lindroos, A. Bansil, H. Ding, D. Koelling, and B. Dabrowski, Phys. Rev. Lett. **73**, 3302 (1994).
- [25] J. Ma, C. Quitmann, R. J. Kelley, P. Almeras, H. Berger, G. Margaritondo, and M. Onellion, Phys. Rev. B **51**, 3832 (1995).
- [26] T. Timusk and B. Statt, *Rep. Prog. Phys.* **62**, 61 (1999).
- [27] H. Ding, T. Yokaya, J. C. Campuzano, T. Takahashi, M. Randeria, M. R. Norman, T. Mochiku, K. Kadowaki, and J. Giapinzakis, *Nature* **382**, 51 (1996).
- [28] S. H. Blanton, R. T. Collins, K. H. Kelleher, L. D. Rotter, Z. Schlesinger, D. G. Hinks, and Y. Zheng, Phys. Rev. B **47**, 996 (1993).
- [29] M. A. Karlow, S. L. Cooper, A. L. Kotz, M. V. Kelvin, P. D. Han, and D. A. Payne, Phys. Rev. B **48**, 6499 (1993).
- [30] Hyun-Tak Kim, H. Uwe, and H. Minami, *Advances in Superconductivity VI* (Springer-Verlag, Tokyo, 1994), P. 191.
- [31] J. L. Tallon and J. W. Loram, *Physica C* **349**, 53 (2001).
- [32] Hyun-Tak Kim, *Physica C* **341-348**, 259 (2000):cond-mat/0001008:cond-mat/0104055.
- [33] T. M. Rice and L. Sneddon, Phys. Rev. Lett. **47**, 689 (1981).
- [34] Hyun-Tak Kim, Phys. Rev. B **54**, 90 (1996).
- [35] J. W. Loram, K. A. Mirza, J. R. Cooper, W. Y. Liang, and J. M. Wade, *Journal of Superconductivity* **7**, 243 (1994).
- [36] J. W. Loram, J. L. Luo, J. R. Cooper, W. Y. Liang, and J. L. Tallon, *Physica C* **341-348**, 831 (2000).
- [37] A. Junod, D. Eckert, T. Graf, G. Triscone, and J. Muller, *Physica C* **162-164**, 482 (1989).
- [38] A. M. Gabovich, A. I. Voitenko, J. F. Annett, and M. Ausloos, *Supercond. Sci. Technol.* **14**, R1 (2001).
- [39] Tohr Ogawa, Kunihiko Kanda, and Takeo Matsubara, *Prog. Theor. Phys.* **53**, (1975) 614.
- [40] Dieter Vollhardt, *Rev. Mod. Phys.* **56**, (1984) 99.
- [41] Patrick Fazekas, *Lecture Notes on Electron Correlation and Magnetism*, Chapter 9, (World Scientific Co., 1999).
- [42] T. Moriya, *BUTSURI* (edited by Physical Society of Japan), Vol 54, No. 1, (1999) 48 (Japanese).
- [43] H. Fukuyama, M. Imada, and T. Moriya, *BUTSURI* (edited by Physical Society of Japan), Vol 54, No. 2, (1999) 123 (Japanese).
- [44] M. N. Khan, Hyun-Tak Kim, H. Minami, and H. Uwe, *Materials Letters* **47**, 95 (2001).
- [45] J. S. Ahn, J. Bak, H. S. Choi, T. W. Noh, J. E. Han, Yunkyu Bang, J. H. Cho, and Q. X. Jia, Phys. Rev. Lett. **82**, 5321 (1999).
- [46] A. Georges, G. Kotliar, W. Krauth, and M. J. Rozenberg, *Rev. Mod. Phys.* **68**, 13 (1996).
- [47] Y. Hongshun, Z. Xiaonong, Z. Changfei, W. Keqin, C. Liezhao, C. Zhaojia, *Physica C* **172**, 71 (1990).
- [48] Manfred Daümling, *physica C* **183**,293 (1991).

- [49] H. Wühl, R. Benischke, M. Braun, B. Frank, O. Kraut, R. Ahrens, G. Bräuchle, H. Claus, A. Erb, W. H. Fietz, C. Meingast, G. Müller-Vogt, and T. Wolf, *Physica C* **185-189**, 755 (1991).
- [50] J. L. Smith, C. M. Fowler, B. L. Freeman, W. L. Hults, J. C. King, and F. M. Mueller, *Advances in superconductivity III*, (Springer-Verlag, Tokyo, 1991), p. 231.
- [51] N. Toyota, T. Sasaki, K. Murata, Y. Honda, M. Tokumoto, H. Nando, N. Kinoshita, H. Anzai, T. Ishiguro, and Y. Muto, *J. Phys. Soc. Japan* **57**, 2616 (1988).
- [52] K. Oshima, H. Urayama, H. Yamochi, and G. Saito, *Physica C* **153-155**, 1148 (1988).
- [53] D. S. Dessau, Z.-X. Shen, D. M. King, D. S. Marshall, L. W. Lombardo, P. H. Dickinson, A. G. Loeser, J. DiCarlo, C. H. Park, A. Kapitulnik, and W. E. Spicer, *Phys. Rev. Lett.*, **71**, 2781 (1993).
- [54] Y. D. Chuang, A. D. Gromko, D. S. Dessau, Y. Aiura, Y. Yamaguchi, K. Oka, A. J. Arko, J. Joyce, H. Eisaki, S. I. Uchida, K. Nakamura, and Yoichi Ando, *Phys. Rev. Lett.* **83**, 3717 (1999).
- [55] A. D. Gromko, Y. D. Chuang, D. S. Dessau, K. Nakamura, and Yoichi Ando, *cond-mat/0003017*.